catalysts

MDPI

Article

Synergistic Effect in Au-Cu Bimetallic Catalysts for the Valorization of Lignin-Derived Compounds

Marta Stucchi [1], Sofia Capelli [1], Simone Cardaci [1], Stefano Cattaneo [1], Andrea Jouve [1], Andrea Beck [2], György Sáfrán [3], Claudio Evangelisti [4], Alberto Villa [1] and Laura Prati [1,*]

1 Chemistry Department, University of Milan, Via Golgi 19, 20133 Milan, Italy; marta.stucchi@unimi.it (M.S.); sofia.capelli@unimi.it (S.C.); simone.cardaci@studenti.unimi.it (S.C.); stefano.cattaneo2@unimi.it (S.C.); andrea.jouve@unimi.it (A.J.); alberto.villa@unimi.it (A.V.)
2 Centre for Energy Research, Surface Chemistry and Catalysis Department, P.O. Box 49, H-1525 Budapest, Hungary; beck.andrea@energia.mta.hu
3 Centre for Energy Research, Institute for Technical Physics and Materials Science, P.O. Box 49, H-1525 Budapest, Hungary; safran.gyorgy@energia.mta.hu
4 National Research Centre (CNR)-Istituto di Chimica dei Composti Organometallici, Via G. Moruzzi, 1, 56124 Pisa, Italy; claudio.evangelisti@cnr.it
* Correspondence: laura.prati@unimi.it; Tel.: +39-02503-14357

Received: 14 February 2020; Accepted: 13 March 2020; Published: 16 March 2020

Abstract: The selective oxidation of veratryl alcohol as lignin-derived compound was studied under mild conditions, using Au-Cu catalysts synthesized from pre-formed nanoparticles with different Au:Cu molar ratios. Bimetallic catalysts show higher activity compared to monometallic counterparts, highlighting a clear synergistic effect. By comparing the physico-chemical surface properties of catalysts supported on carbon and Al_2O_3, we were able to establish a strong support effect, with alumina-based catalysts being more active than carbon-supported ones. Moreover, TEM and X-ray photoelectron spectroscopy (XPS) analyses showed a different composition of nanoparticles (NPs) and metal exposure, and we established that Au is the active phase of the reaction. The co-presence of Au and Cu species, and their different interaction with the support, enabled obtaining more than 70% conversion of veratryl alcohol to veratryl aldehyde as a unique product. Moreover, the Au_1Cu_1 supported on alumina catalyst was recovered by filtration and reused without significant loss of activity and selectivity up to four times.

Keywords: veratryl alcohol; veratraldehyde; Au-Cu bimetallic catalysts; support effect; catalytic oxidation; second-generation biomass

1. Introduction

The transformation of biomass into fuel and chemicals is becoming increasingly essential as a way to mitigate global warming and diversify energy sources. Biomass is indeed a renewable and carbon-neutral resource. Moreover, it has been estimated that biomass could provide about 25% of global energy requirements, as well as being a source of valuable chemicals, pharmaceuticals and food additives. Second-generation biomass is mainly composed of cellulose, hemicellulose and lignin. After cellulose, lignin is the second most abundant natural polymer. The aromatic rich structure of lignin has a potential as a feedstock for the production of organic chemicals. However, while designated applications for cellulose already exist, sustainable ways to valorise lignin are yet to be established [1]. Lignin-derived compounds containing significant linkages are commonly used for a better understanding of its catalytic valorisation [2]. Their liquid phase oxidation is a core unit process for producing a variety of fine chemicals [3], with particular interest in the selective oxidation of side

chain hydroxyl-group of substituted aromatics to aldehydes. Indeed, the selective oxidation of alcohols to the corresponding aldehydes, ketones or acids finds its importance in the pharmaceutical industry as well as in the large-scale chemical industry [4]. Veratryl alcohol (VA) (Figure 1) is a lignin-derived compound, obtained during delignification process in water medium [5].

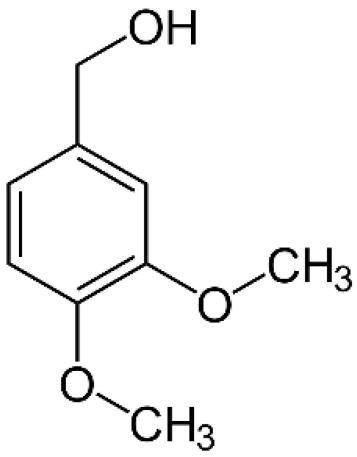

Figure 1. 3,4-dimethoxy benzyl alcohol (veratryl alcohol) molecular structure.

It is used to study the chemical transformation of lignin-derived compounds for the production of biofuels and aromatic chemicals [6]; in particular, VA could be selectively oxidized to veratrylaldehyde (VAld) in the presence of enzymatic catalysts [7], but the high cost and poor stability of the enzymes severely limit their practical application. However, veratraldehyde is desired, being widely used as a flavouring agent and as an important pharmaceutical intermediate for drugs [8].

The oxidation of benzylic system is often reported in the literature, but most of the results are obtained by homogeneous catalysts, which requires the presence of NaOH, phosphate buffer and stoichiometric amount of oxidizing agents [9]. Homogeneous catalysts are disadvantageous, requiring multistep synthesis, often showing fast deactivation and being difficult to recover. For this reason, many researchers investigated the catalytic oxidation on biomass model compounds by heterogeneous catalysis; in fact, the catalytic oxidation of veratryl alcohol by heterogeneous catalysts has already been reported [10,11]. Nevertheless, high conversions and selectivity were obtained only under harsh reaction conditions. For example, Rode et al. [10] reported the aqueous phase catalytic oxidation of veratryl alcohol by a nano-structured Co_3O_4 catalyst, showing a conversion of 85% with 96% selectivity to veratrylaldehyde, where the reaction was carried out at 140 °C and 40 bar of O_2. Moreover, the preparation of the catalyst required continuous stirring for 12 h at 70 °C and a calcination step at 300 °C for 5 h. Riisager et al. [11] reported the oxidative transformation of VA to veratrylaldehyde (VAld) with air, by Ru supported on γ-alumina or silica: also in this case, the reaction conditions used were harsh, i.e., temperature above 150 °C and pressure higher than 3 bar. Additionally, the catalysts needed to be calcined at 450 °C for 6 h.

More recently, Prati et al. [12] reported the oxidation of a lignin model structure including veratryl alcohol at rather mild conditions by Au-Pd on active carbon catalysts. The oxidation of veratryl alcohol was performed at 80 °C and 2 bar of oxygen, for comparison with the oxidation of benzyl alcohol and 1-methoxy-benzyl alcohol. Despite Au-Pd catalysts converting VA to VAld with 100 % selectivity, the maximum conversion achieved in 6 h was just 30% with an initial activity of 151 h^{-1} (mol converted per mol of metal per hour). In fact, the presence of the methoxy-groups on the aromatic rings led to a strong decrease of activity compared to that obtained in the benzyl alcohol oxidation, due to an irreversible adsorption of the substrate on the metal active site increased by the methoxy-group. At the same time, Chen et al. reported the selective oxidation of veratryl alcohol over Au-Pd supported on ceria-zirconia [13], obtaining a veratryl alcohol conversion of 72% and selectivity toward VAld of

99%. Thus, comparing the results obtained with different supports, it is presumable that the oxidation of veratryl alcohol is support-sensitive, where metal oxide supports may have a strong effect on the catalytic activity.

Considering the metal active species, gold-based catalysts are widely exploited for the oxidation of a variety of hydrocarbons and alcohols [14–16]. Differently from Pt or Pd, Au showed high selectivity and high resistance to O_2-poisoning [17], but usually a lower activity. Au-based bimetallic catalysts, however, often showed improved catalytic activity (synergistic effect) and a combination of the properties of the two constituting metals [18].

Copper has been reported to catalyse oxidation of alcohols [19], even presenting quite low conversion, considering the advantage to be an alternative to the more expensive conventional precious metals [20]. It has been shown that the combination of other metals is beneficial. Indeed, although monometallic Cu did not show a good activity for alcohols oxidation, many works have reported a synergistic effect between gold and copper in oxidation reactions [21,22]. In particular, the oxidation of benzyl alcohol has been reported by M. Rossi et al. [23], using mono- and bimetallic gold–copper on silica catalyst and proving that the bimetallic Au–Cu/SiO_2 catalyst led to benzaldehyde in over 98% yield. More recently, C. Evangelisti et al. [24] reported the catalytic activity of some hybrid Au/CuO nanoparticles (NPs) supported on carbon for the catalytic liquid-phase selective benzyl alcohol oxidation, demonstrating a strong synergistic effect of Au/CuO heterostructures.

Some examples are also reported for the CO oxidation. Liu et al. [25] reported Au-Cu NPs supported on SBA-15, showing higher activity in CO oxidation than the corresponding monometallic counterparts; the active catalyst was composed of Au NPs enriched on the surface by partially or fully oxidized CuOx, which boosted the CO/O_2 activation. Again, J. Yin et al. [25] reported the CO oxidation promoted by carbon-supported Au-Cu catalysts, where the reduction treatment by hydrogen of the calcined catalyst led to the formation of oxygenated Cu species at the NPs' surface, able again to activate oxygen with an increase of the catalytic activity.

Here, we investigated the possible synergistic effect between Au and Cu at different metal ratio in VA oxidation under mild conditions. The aim of this study is to reduce the presence of precious metals such as gold but also to find a robust catalyst to be applied in VA oxidation. The support effect has been also investigated by using alumina and active carbon as supports.

2. Results and Discussion

2.1. Catalyst Characterization

2.1.1. Energy Dispersive X-Ray (EDX) and UV-vis Spectra of the Parent Sols

The characterization of sols has been performed before their immobilization on the supports. Particular attention was paid to particle composition that normally constitutes a big challenge in bimetallic catalysts. We investigated different Au:Cu molar ratios, namely 4:1, 1:1 and 1:4.

In Au_1Cu_1 sol, the Au and Cu elemental maps (Figure 2) well demonstrated the co-existence of the two metals in the single particles. The Au/Cu atomic ratio varied between 44/66 and 61/39 according to the quantification of the EDS spectra collected on nine particles (the quantified error of the Au and Cu atomic concentrations was about 20%).

In the Au_4Cu_1 (Figure 3) and Au_1Cu_4 sols (Figure 4), bimetallic particles were also clearly detected by the elemental maps, although in small size particles high enough intensities could hardly be gained, especially for the lower concentrated component. The Au_1Cu_4 contained a high population of smaller low Au content (< 15 atomic %) bimetallic or monometallic Cu(Ox) particles, in addition to some larger particles of an Au/Cu atomic ratio between 52/48 and 78/22. In the case of Au_4Cu_1 sol, particles with different atomic composition in the range of Au/Cu = 48/52 and 85/15 were detected.

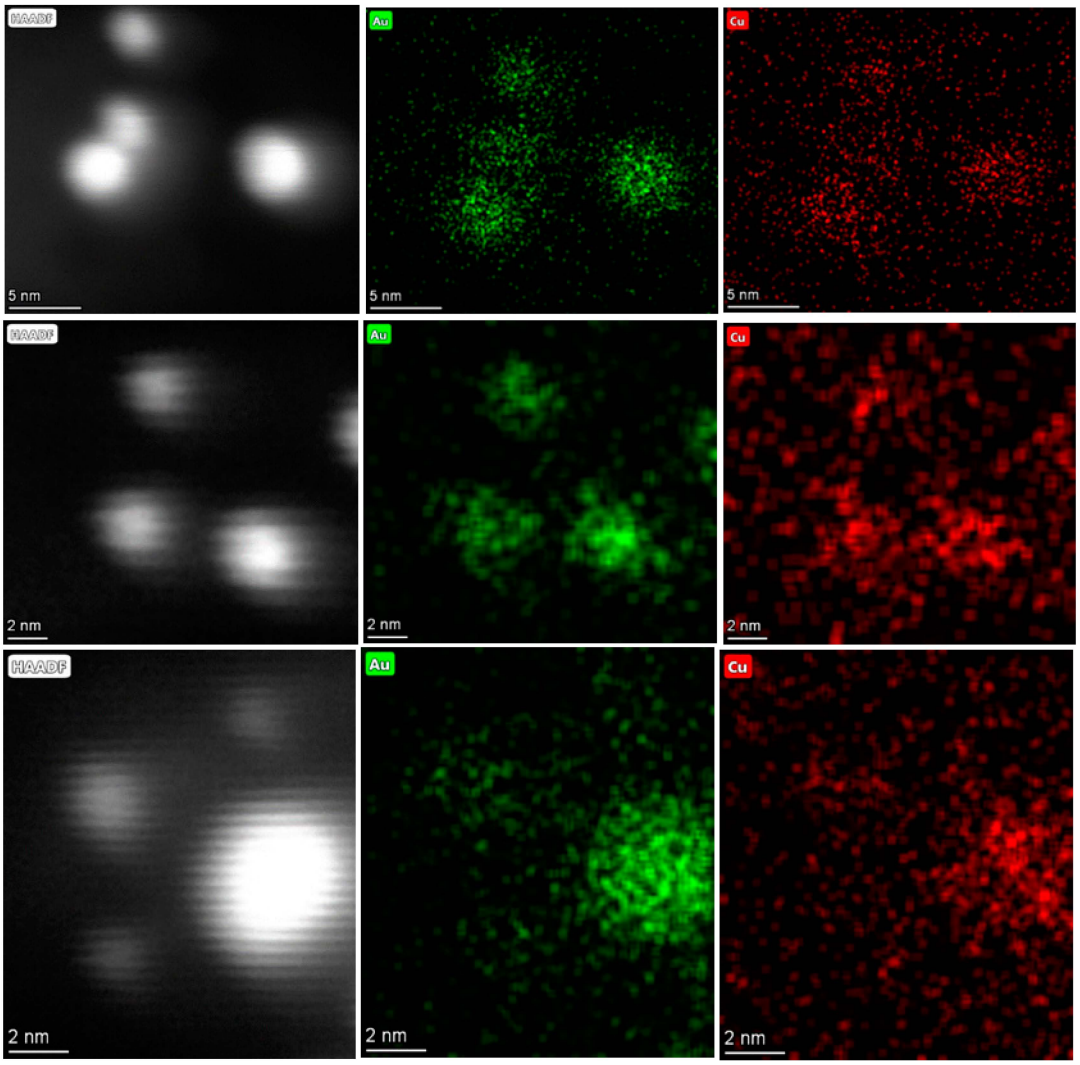

Figure 2. High angular annular dark field (HAADF) images with Au and Cu elemental maps (background corrected and fit Au-L and Cu-K intensities, respectively) recorded during the STEM-EDS measurement of Au1Cu1 sol.

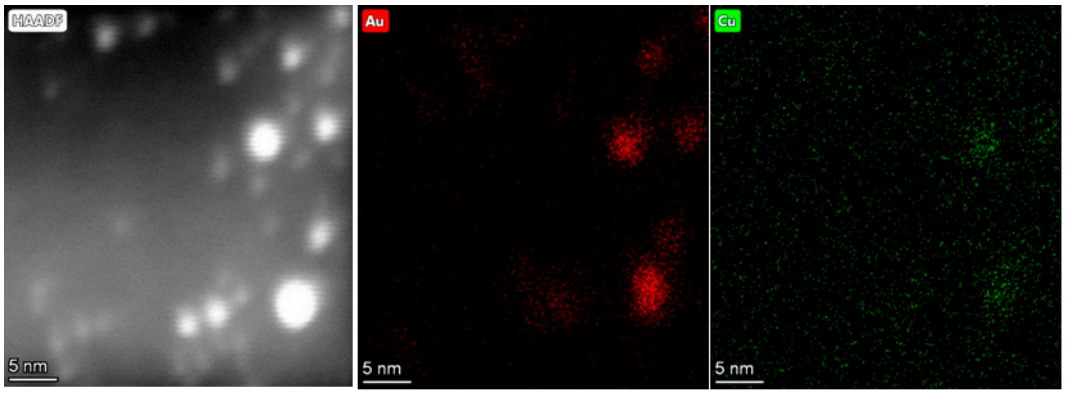

Figure 3. *Cont.*

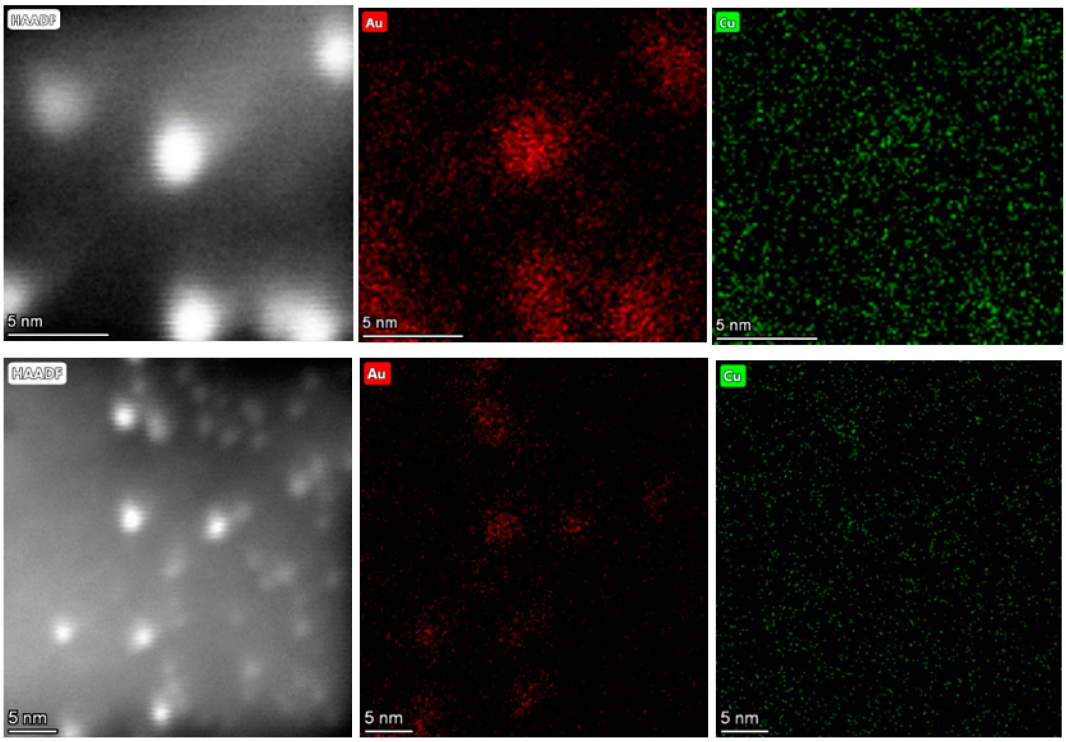

Figure 3. HAADF image with Au and Cu elemental maps (background corrected and fit Au-L and Cu-K intensities, respectively) recorded during the STEM-EDS measurement of Au_4Cu_1 sol.

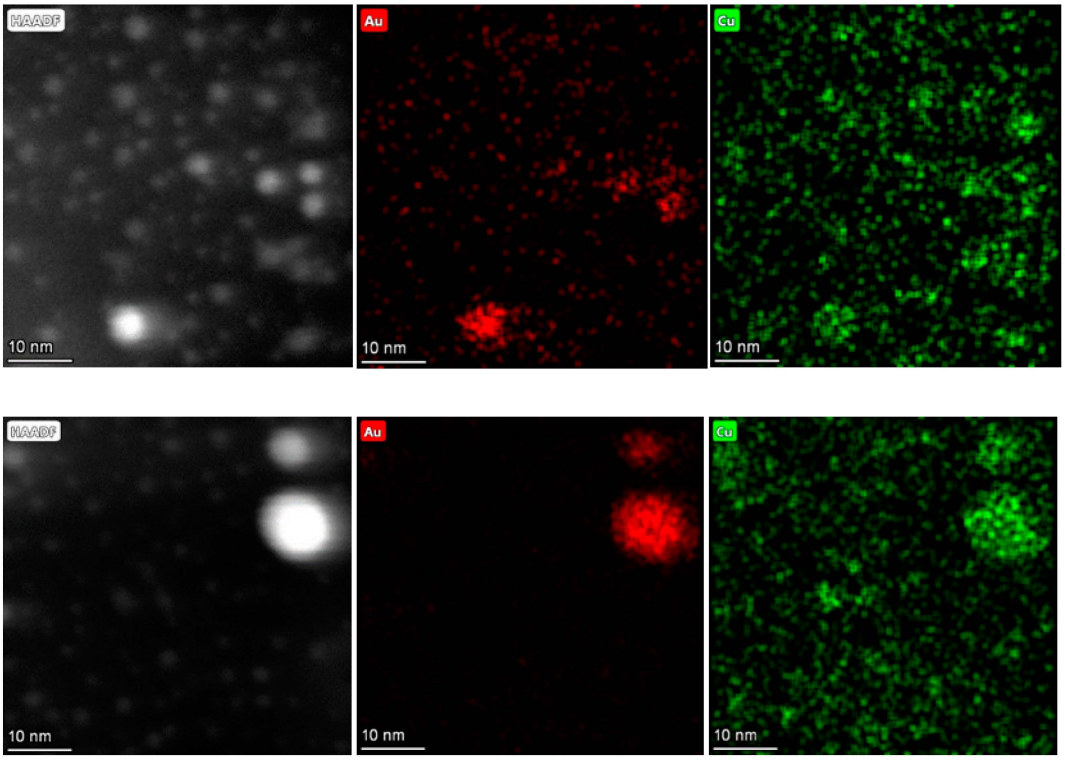

Figure 4. HAADF image with Au and Cu elemental maps (background corrected and fit Au-L and Cu-K intensities, respectively) recorded during the STEM-EDS measurement of Au_1Cu_4 sol.

The UV-vis spectra of the parent sols of the different samples are depicted in Figure 5a. The localized surface plasmon resonance (LSPR) bands of the plasmonic Au and Cu containing metal nanoparticles

located in the 450–700 nm spectrum range are very weak due to the small particle size of around 2 nm [26]. For better visibility, the LSPR bands were baseline corrected and enlarged (Figure 5b). The wavelength of the plasmon band of the monometallic Au sol at 516 nm agrees well with the literature. A characteristic band of Au NP dispersion appears at about 520 nm [27]. The weak wide band at 632 nm in the case of monometallic Cu sol may be attributed to Cu NPs with CuOx shell formed due to the facile oxidation of Cu NPs even at room temperature on air contact. The metallic Cu NPs are characterized by a plasmon resonance centred at 570–580 nm, that strongly broadens for particles below 4 nm [28,29]. The formation of surface Cu_2O and the thickening of this oxide shell induces a continuous red shift and a decreasing of intensity by increasing the depth of the oxidized layer [30]. The latter oxidation of Cu is delayed in alloyed AuCu particles, as reported in ref. [31]. The plasmon peaks of the Au_4Cu_1, Au_1Cu_1 and Au_1Cu_4 in bimetallic sols appeared at 533, 562 and 578 nm, presenting increasing red shift compared to the Au peak towards that of Cu. The observed plasmon band of Au_4Cu_1 is roughly linearly red-shifted from that of a monometallic Au in proportion to the increase in the mol fraction of Cu, suggesting alloyed particles (disordered alloy formation is assumed). However, for the Au_1Cu_1 and Au_1Cu_4 sols, these shifts are larger than expected due to alloying. We suppose oxidation of surface copper in these cases, resulting in additional red shift.

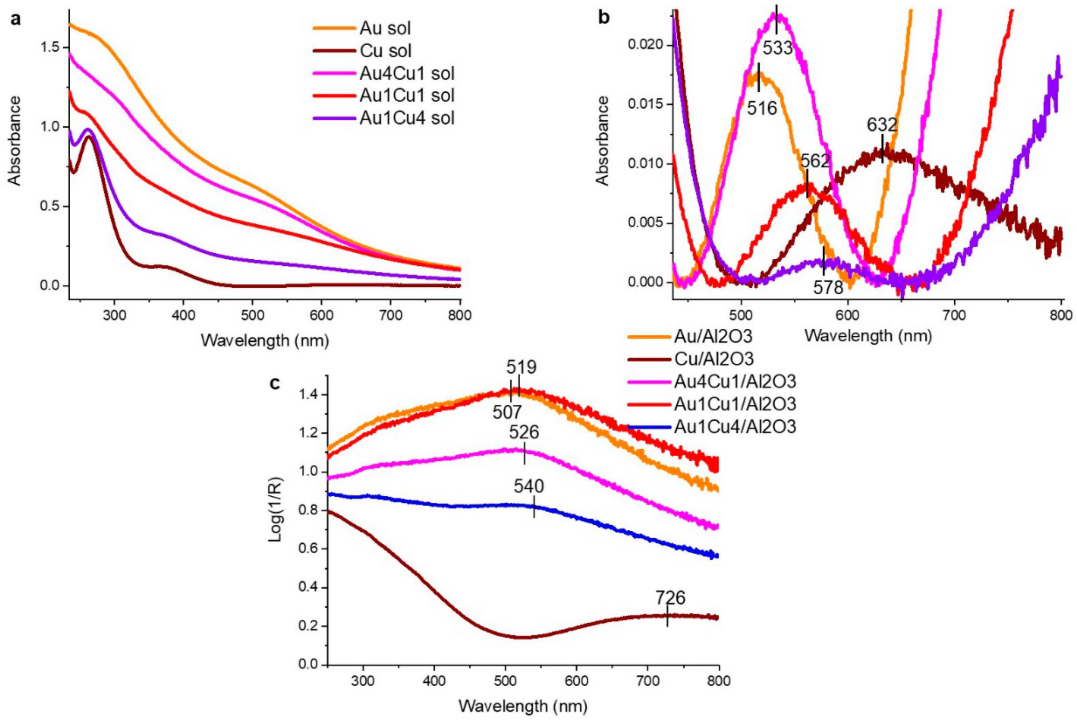

Figure 5. UV-vis spectra of the parent sols (**a**), the same spectra base line corrected in the localized surface plasmon resonance (LSPR) region (**b**) and of supported catalysts (**c**).

In the spectra of sols immobilized on alumina (see Figure 5c), wide weak bands are visible. In the case of the Au-containing samples, the LSPR bands blue shifted relative to those of the corresponding sols, and the difference between them reduced. In Cu/Al_2O_3, the catalyst copper is presumably oxidized. Unfortunately for catalysts supported on carbon, UV-Vis analyses can hardly be carried out due to their low reflection.

2.1.2. ICP-OES (Inductively Coupled Plasma Optical Emission Spectroscopy) Measurements

The ICP-OES analyses performed on the supported NPs confirmed the trend revealed by the EDX mapping of the particles: Au-rich catalyst appeared richer than the nominal value, while the Cu-rich catalyst was more rich in copper with respect to the nominal value. ICP-OES was performed using

a ICP Perkin Elmer optical emission spectrometer Optima 8000 for measuring the actual loading of metal and actual ratio between Au and Cu. Au-Cu-supported samples were dissolved using a CEM MARS One Microwave Digester, using an acidic solution of HCl (37%) and H_2SO_4 (98%) at 180 °C for alumina-supported samples, and using a sulfonitric mixture (HNO_3:H_2SO_4 1:3) for carbon supported ones. Au was dissolved by aqua regia (HNO_3:HCl 1:3).

More details about the methodology for catalyst digestion are reported in the Experimental Section. The results are reported in Table 1. The experimental metal loadings are in agreement with the nominal values within the experimental error. The actual Au/Cu ratio values are in good agreement with the nominal values considering that the major component is always present in a slightly higher amount with respect to the nominal value: the Au_4Cu_1 appears more rich in Au, whereas Au_1Cu_4 is more rich in Cu.

Table 1. Nominal and actual metal loadings obtained by inductively coupled plasma (ICP) analyses.

Catalyst	Loading wt. %		Au/Cu mol/mol	
	Nominal	Actual	Nominal	Actual
Au/Al_2O_3	3.0	2.7	-	-
Au_4Cu_1/Al_2O_3	2.6	2.2	4.00	3.61
Au_1Cu_1/Al_2O_3	2.0	1.8	1.00	0.88
Au_1Cu_4/Al_2O_3	1.4	1.2	0.25	0.33
Cu/Al_2O_3	1.0	1.4	-	-
Au/C	3.0	2.9	-	-
Au_4Cu_1/C	2.6	2.2	4.00	3.64
Au_1Cu_1/C	2.0	1.9	1.00	0.97
Au_1Cu_4/C	1.4	1.5	0.25	0.26
Cu/C	1.0	1.1	-	-

2.1.3. XPS Analyses

In order to investigate the nature of surface species and their oxidation state, we used X-ray photoelectron spectroscopy (XPS) which was performed on all the supported bimetallic catalysts (Table 2).

Table 2. X-ray photoelectron spectroscopy (XPS) high-resolution spectra and survey analyses of C- and Al_2O_3-supported catalysts.

		Survey			HR						
					Au $4f_{7/2}$						
		Au (%At)	Cu (%At)	Au/Cu	Au^0	$Au^{\delta+}$	Cu^0-Cu^+	CuO	$Cu(OH)_2$	$Cu(NO_3)_2$	Sat.
Au_4Cu_1/C	*B.E. (eV)*				84.3	85.5	-	933.9	-	-	
	%At	0.19	0.03	6.3	77	23	-	100	-	-	yes
Au_1Cu_1/C	*B.E. (eV)*				84.4	85.4	932.2	-	-	935.8	
	%At	0.10	0.11	0.91	74	26	65	-	-	35	-
Au_1Cu_4/C	*B.E. (eV)*				83.3	-	932.9	-	934.5	-	
	%At	0.07	0.09	0.77	100	-	78	-	22	-	-
Au_4Cu_1/Al_2O_3	*B.E. (eV)*				83.5	85.7	-	934.0	-	-	
	%At	0.97	0.53	1.83	78	22	-	100	-	-	yes
Au_1Cu_1/Al_2O_3	*B.E. (eV)*				83.5	86.1	932.9	-	-	935.6	
	%At	0.64	0.84	0.76	83	17	61	-	-	39	-
Au_1Cu_4/Al_2O_3	*B.E. (eV)*				83.7	-	932.7	-	934.6	-	
	%At	0.16	1.36	0.12	100	-	70	-	30	-	-

The Au/Cu ratio evaluated from survey spectra shows that in the carbon-supported catalysts, only in the case of Au_1Cu_1, the surface composition is around 1, whereas in both Au-rich and Cu-rich catalysts we observed a surface enrichment of Au; in all three alumina-supported samples, Cu was enriched on the surface compared to the bulk composition.

From high-resolution spectra (HR) of Au $4f_{7/2}$, two main species were clearly detected: Au^0 (83.5–84.4 eV) and $Au^{\delta+}$ (85.4–86.1 eV). Au^0 was always the main component and for C-supported samples its amount was 74% and 77% for Au_1Cu_1 and Au_4Cu_1, respectively. Instead, for Al_2O_3-supported

catalysts the Au^0 amount is higher: 83% and 78% for Au_1Cu_1 and Au_4Cu_1 samples, respectively. Of particular interest is the presence of 100% of Au^0 in Au_1Cu_4 samples both on carbon and Al_2O_3 support.

Regarding the HR of Cu $2p_{3/2}$, four main components were detected, even if it was impossible to separate the contribution of Cu^0 and Cu^+. Cu^0-Cu^+ was detected at 932.2–932.9 eV, CuO at 933.9–934.0 eV and $Cu(OH)_2$ at 934.5–934.6 eV. Au_4Cu_1 samples show the presence of only CuO with the satellite peak of Cu^{II}, which is, however, not possible to quantitatively evaluate due to the low signal intensity. In Au_1Cu_1 samples, Cu^0-Cu^+ was detected in similar amounts: 65% and 70% on carbon and Al_2O_3, respectively. Moreover, these two samples also show the presence of a peak which could be tentatively assigned to $Cu(NO_3)_2$, which was the metal precursor used during the synthesis of the sol. However, although the deconvolution seems to point out the presence of a peak, the assignment to $Cu(NO_3)_2$ appears uncertain as the catalyst was repeatedly washed, thus assuring the removal of residual copper nitrate. Moreover, this peak is visible only in the case of Au1Cu1 catalyst and no evidence of a satellite peak of Cu(II) is present.

Finally, Au_1Cu_4 samples revealed the presence of Cu^0-Cu^+ and $Cu(OH)_2$, being the first one the main species. The presence of Cu^{II} in the catalysts prepared with a low amount of Cu is possibly the result from the redox reaction between Cu^0 and Au $^{\delta+}$ [32]. Therefore, in these samples, most of Cu probably underwent this reaction. On the other hand, when Cu is present in a large amount with respect to Au, the internal redox can be stopped and it can remain as Cu^0 or passivated by air.

2.1.4. High Angular Annular Dark Field Scanning Transmission Electron Microscopy (HAADF-STEM)

The particle size distribution and dispersion of the metallic particles of AuCu bimetallic catalysts was investigated by HAADF-STEM. Representative micrographs of the bimetallic AuCu catalysts supported on alumina and carbon are reported in Figures 6 and 7, respectively, together with their particle size distribution.

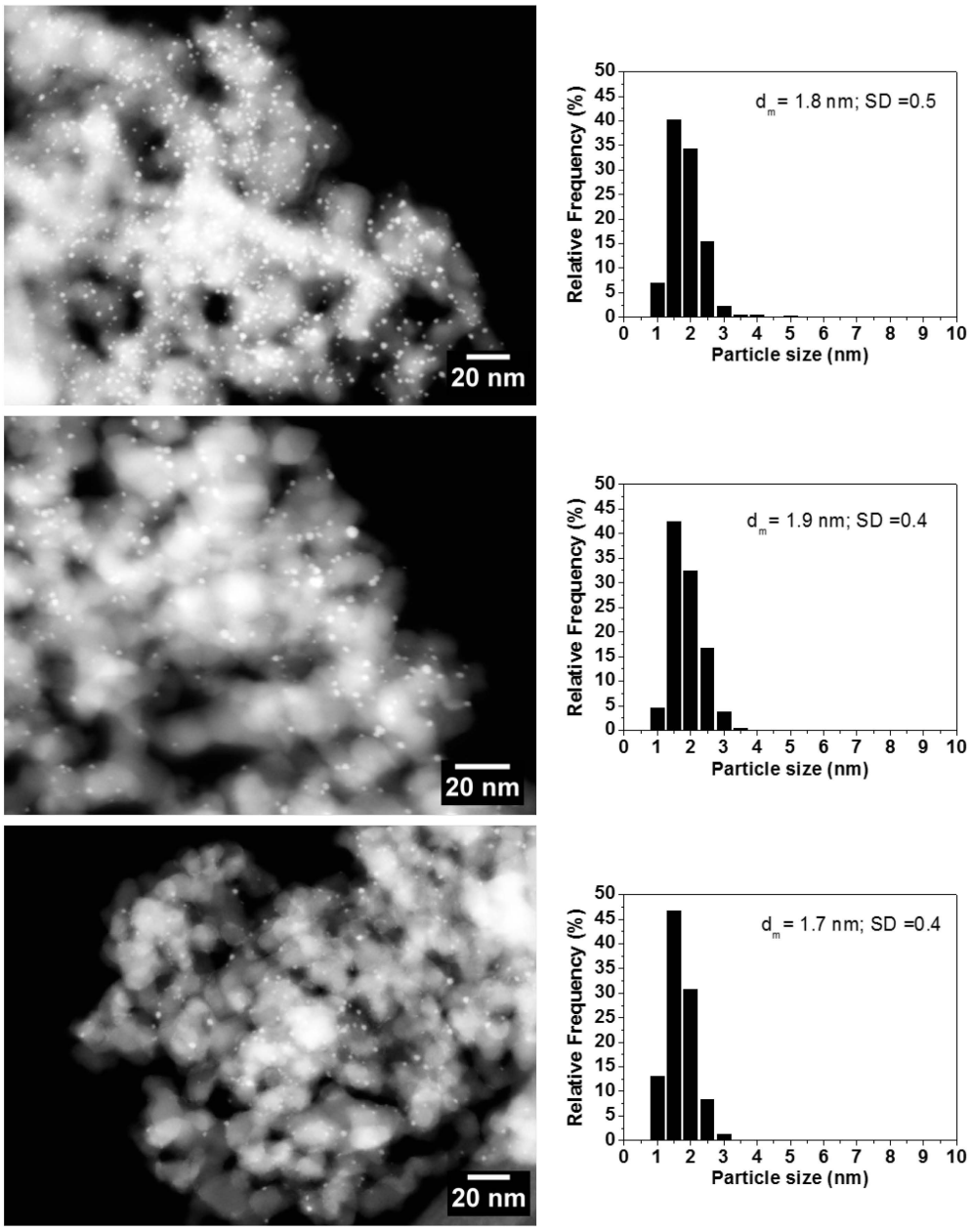

Figure 6. Representative HAADF-scanning transmission electron microscopy (STEM) micrograph and particle size distribution of Au_4Cu_1/Al_2O_3 (top), Au_1Cu_1/Al_2O_3 (middle), Au_1Cu_4/Al_2O_3 (bottom).

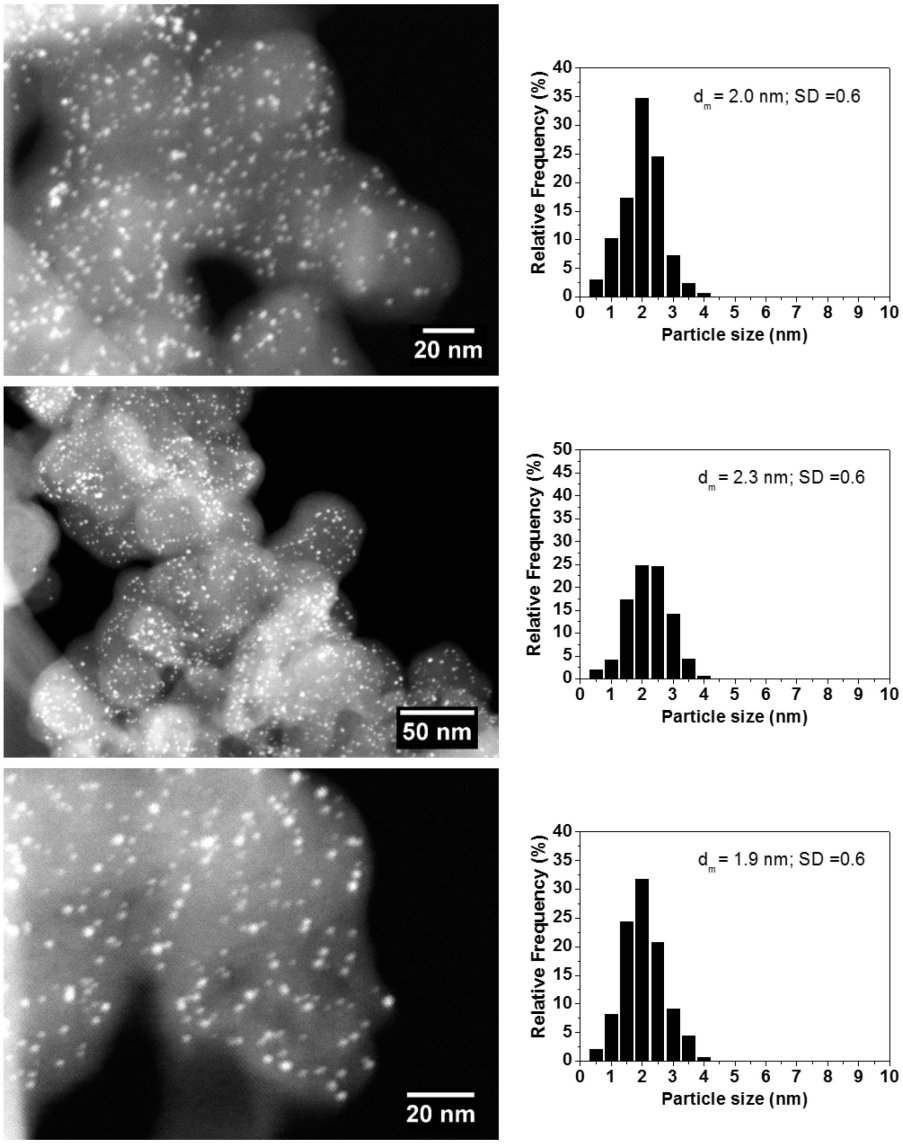

Figure 7. Representative HAADF-STEM micrograph and particle size distribution of Au_4Cu_1/C (top), Au_1Cu_1/C (middle), Au_1Cu_4/C (bottom).

In all the bimetallic samples, a high metal dispersion was observed. Alumina-supported AuCu bimetallic samples (Figure 6) showed very similar particle size (d_m = 1.7–1.9 nm) and distributions, regardless the AuCu molar ratio.

In the carbon-supported AuCu bimetallic catalysts (Figure 7), the support appeared densely populated by nanometric metal particles. The Au/Cu molar ratio did not significantly affect the particle sizes which showed a slight increase with respect to the alumina-supported samples (d_m 1.9 nm–2.3 nm).

2.2. Catalytic Behaviour

Testing all the carbon-supported catalysts in VA oxidation at 80 °C and 2 bar of oxygen pressure (Figure 8), we observed a negligible activity, reaching, in all cases, conversions of < 10% after 6 h. Notably, the monometallic Cu/C was completely inactive. This was not unexpected as in the literature it has been reported that the Cu species are unable to activate O_2 and they do not act as active sites [25].

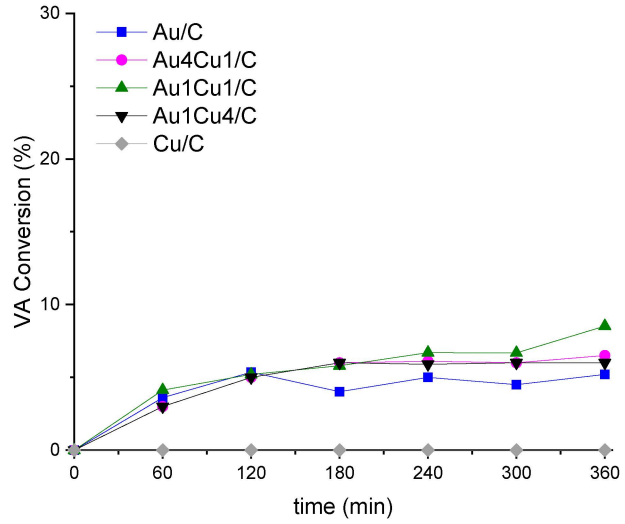

Figure 8. Veratryl alcohol (VA) conversion as a function of reaction time by Au, Cu and Au-Cu supported on carbon. Reaction conditions: 80 °C, 2 bar of O_2, VA 0.15 M in p-xylene, VA: metal molar ration 1000:1.

A strong support effect could be hypothesized by comparing carbon-supported catalysts with alumina-supported ones (Figure 9). Au_4Cu_1/Al_2O_3 reached 70% conversion of VA with respect to less than 10% obtained by the same composition supported on carbon. As in the case of Cu/C, monometallic Cu supported on Al_2O_3 did not show any activity.

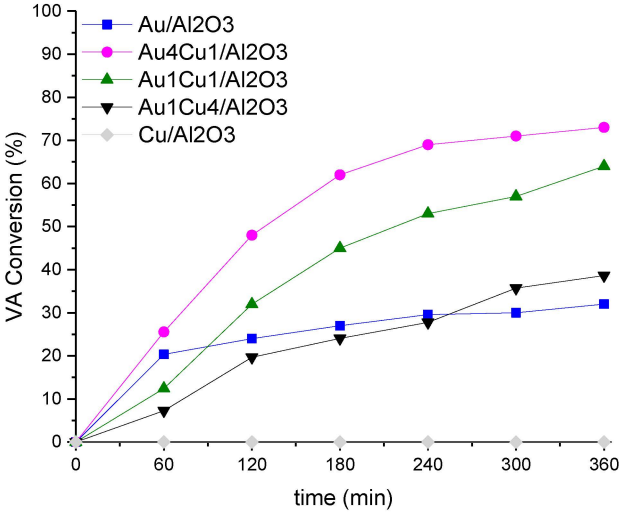

Figure 9. VA conversion as a function of reaction time by Au- and Au-Cu supported on alumina. Reaction conditions: 80 °C, 2 bar of O_2, VA 0.15 M in p-xylene, VA: metal molar ration 1000:1.

In terms of initial activity (defined as mol converted per mol of metal per hour), Au/Al_2O_3 showed an initial activity of 200 h^{-1} (Figure 10) and converted 30 % of VA in 6 h (Figure 9). The initial activity for Au_4Cu_1/Al_2O_3, Au_1Cu_1/Al_2O_3 and Au_1Cu_4/Al_2O_3 are, respectively, 250, 120 and 60 h^{-1}. On the basis of these data, we could suppose the presence of a slight synergistic effect considering the decreased amount of Au. However, looking at the reaction profile reported in Figure 9, it clearly appears that bimetallic catalysts showed an improved resistance to deactivation with respect to Au/Al_2O_3, which tends to deactivate after 1 h of reaction. On this aspect, the catalyst which shows the higher resistance appears to be the Au_1Cu_1/Al_2O_3 (green line in Figure 9).

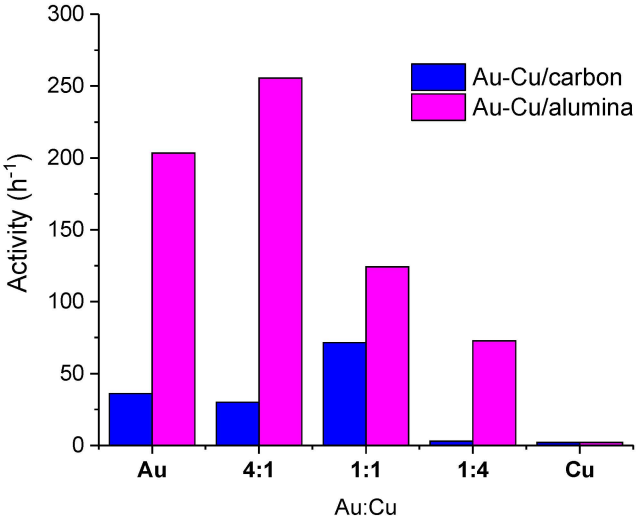

Figure 10. Initial activity (h^{-1}) (mol converted per mol of metal per hour) calculated at 1 h of reaction as a function of the Au/Cu molar ratio. Comparison between alumina- and carbon- supported Au and Au-Cu catalysts.

Comparing the initial activity of Al_2O_3- and C-supported catalysts (Figure 10) we could note a volcano trend only in the case of the Al_2O_3-supported catalysts. Therefore, copper positively influences the catalyst activity when it is added in low amount.

2.2.1. Correlation of Catalytic Results and Characterization

Considering that supported NPs have a similar particle sizes, we can exclude the effect of this parameter on the catalytic behavior. Contrarily, considering the catalytic results and XPS analyses, we found that the activity is influenced by the support and the catalyst surface composition. The C-supported catalysts show lower Au exposure and lower conversion than the Al_2O_3-supported ones (Figure 11, Table 2). The higher the Au surface exposure, the higher the conversion. Considering the samples Au_4Cu_1/C and Au_1Cu_4/Al_2O_3, with the same Au exposure, we expected the same conversion if the support does not influence the reaction. However, the conversions in these two cases are different (Au_1Cu_4/C 3% and Au_1Cu_4/Al_2O_3 7%—Table 3). Therefore, the choice of the support plays a key role in VA oxidation.

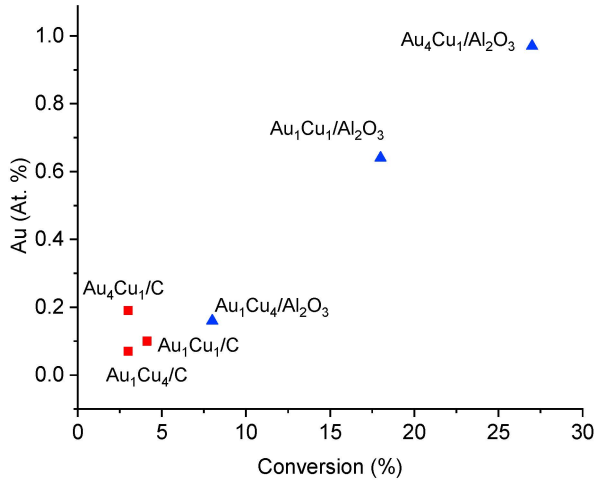

Figure 11. Influence of gold surface exposure on the conversion of VA after 1 h.

Table 3. Amount of exposed metal and gold exposure of Al_2O_3-supported catalysts.

Catalysts	Total Metal Amount (%At.)	Au (%At.)	Au^0 (%At.)	Au^0_{exp} (%At.)	Conversion_1h (%)
Au_4Cu_1/Al_2O_3	1.50	97	78	76	25.6
Au_1Cu_1/Al_2O_3	1.48	64	83	53	12.4
Au_1Cu_4/Al_2O_3	1.52	16	100	16	7.27

Due to the low conversion of C-supported catalyst, we decided to focus our attention on Al_2O_3-supported bimetallic samples and their properties. The total surface metal exposure of these samples is about 1.5 at. % (Table 3, Column 2), but the conversion at 1 h of reaction is very different. These can be ascribed to the presence of different amount of Au and Cu on the catalyst surface. Therefore, the influence of the two metals on VA oxidation was studied (Figure S5). Plotting the Au and Cu surface exposure versus conversion at 1 h of reaction, a linear correlation was established. The higher the amount of exposed Cu, the lower the conversion. Therefore, the Au sites are suggested to be the active sites of the examined reaction which can be modified electronically and also geometrically by interaction and dilution with Cu/Cu-oxide.

To see which is the active phase of the reaction Au^0 amount was considered. Taking into consideration the at. % of Au^0, it seems that the conversion at 1 h of reaction is higher when the amount of metal Au is low. However, through performing a normalization of the Au^0 exposure (Au^0_{exp}) by multiplying the Au^0 at. % (Table 3, column 4) for the Au exposure (Table 3, column 3), more indicative results were obtained (Figure S6). Increasing the amount of exposed Au^0_{exp} the conversion rises linearly. Therefore, we can hypothesize that the active phase in VA oxidation reaction is Au^0.

Moreover, catalytic results reveal that bimetallic catalysts lead to a higher conversion of VA than monometallic Au after 6 h. In fact, the reaction profile of VA oxidation using Au/Al_2O_3 is typical of deactivated catalyst. We can hypothesize that cations of copper maintain the gold in a zero oxidation state at the origin of the synergistic effect, as reported for glycerol oxidation reactions [33].

2.2.2. Stability Tests

Au_4Cu_1 and Au_1Cu_1 supported on alumina showed the highest catalytic activity. Considering the different reaction profiles, which show a higher trend to deactivate in the case of Au_4Cu_1 despite the highest initial activity, we investigated both their life-times by carrying out recycling tests. As reported in Figure 10, Au_4Cu_1 after three runs reduced its activity by about 80%, whereas Au_1Cu_1 shows a pretty good stability (Figure 12).

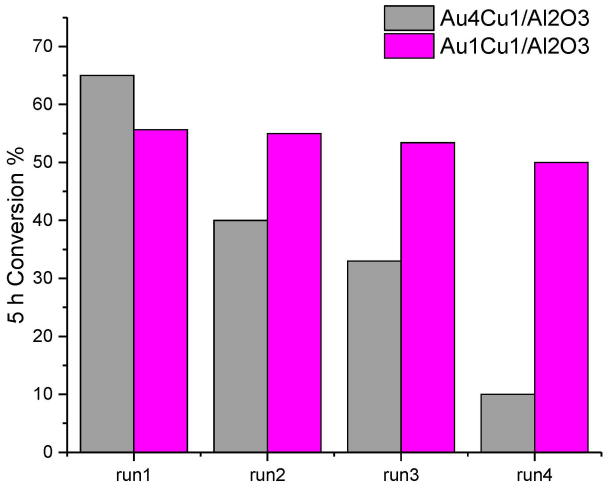

Figure 12. Recycle tests. VA oxidation in p-xylene (0.15 mol L^{-1}), VA: metal molar ratio 1000:1, 80 °C and 2 bar of O_2.

Thus, when copper is present in lower amounts than gold, the catalyst showed a high initial activity, but it tends to deactivate. On the other hand, when increasing the copper content, the stability of the catalytic material increases. ICP-OES measurements showed and confirmed that there is not leaching. Therefore, we ascribed the strong deactivation of Au_4Cu_1/Al_2O_3 to a competitive adsorption of (by)-products on the active site as reported in the literature [34]. By increasing the Cu content in the active phase, it was already observed [35] that there is an increase in stability of the catalytic performances.

3. Materials and Methods

Tetrachloroauric(III) acid trihydrate ($HAuCl_4 \cdot 3H_2O$, 99% and copper(II) nitrate hydrate ($Cu(NO_3)_2 \cdot xH_2O$, 99.999%) were used as precursors for the catalysts synthesis. Sodium borohydride ($NaBH_4$, powder, ≥98.0%) was the reducing agent and polyvinyl alcohol (PVA, MW = 9000–10,000, 80% hydrolysed) was used as the protecting agent. 3,4-dimetoxybenzyl alcohol (99%), veratraldehyde (3,4-dimethoxybenzaldehyde, ≥98%), p-xylene (anhydrous, ≥99%) and undecane (reference standard for GC, Supelco,) were used without any further treatments. All the agents were purchased from Sigma Aldrich/Merck (Darmstadt, Germany).

Aqueous Au-Cu bimetallic and the corresponding monometallic sols of Au/Cu = 1/0, 4/1, 1/1, 1/4 and 0/1 molar ratio were fabricated by co-reduction of $HAuCl_4$ and $Cu(NO_3)_2$ precursors with $NaBH_4$ in the presence of polyvinyl alcohol (PVA) stabilizing agent. To a 685 ml solution of metal precursors (0.33 mM Au + Cu) and PVA (0.013 wt. %) 75 ml of 25.6 mM $NaBH_4$ solution was added suddenly under vigorous stirring in an icy water bath and kept stirring for an hour. Three batches of a given sol were merged and its proper amounts were adsorbed on both alumina (Degussa Aluminium oxide C, 100 m^2/g,) and carbon (VULCAN® XC72R Carbon Black, Cabot, surface area of 218 $m^2\ g^{-1}$, pore volume of 0.41 mL g^{-1}, pore size 10.4 nm, Boston, M.A., USA) [36] supports, providing 0.154 mmol/gcat metal (Au + Cu) loading. The suspension of the sols and supports were stirred overnight at room temperature, then filtered. After thorough washing with ultrapure water, the solids were dried overnight at 80 °C. C indicates the carbon black (Vulcan XC72R) support, while Al_2O_3 is used to name the alumina-supported catalysts. The complete samples list with details is reported in Table 4.

Table 4. Catalysts list, total metal loadings (wt. %) and Au/Cu theoretical molar ratio.

Catalyst Label	Au/Cu Nominal Molar Ratio	Metal Loading, wt. %[a]	AuCu Particle Size, nm[b]
Au/C	-	3	2.7 ± 0.5
Au_4Cu_1/C	4	2.6	2.0 ± 0.6
Au_1Cu_1/C	1	2	2.3 ± 0.6
Au_1Cu_4/C	0.25	1.4	1.9 ± 0.6
Cu/C	-	1	2.9 ± 0.5
Au/Al_2O_3	-	3	2.0 ± 0.5
Au_4Cu_1/Al_2O_3	4	2.6	1.8 ± 0.5
Au_1Cu_1/Al_2O_3	1	2	1.9 ± 0.4
Au_1Cu_4/Al_2O_3	0.25	1.4	1.7 ± 0.4
Cu/Al_2O_3	-	1	2.9 ± 0.5

[a] corresponding to 0.154 mmol metal/g catalyst; [b] mean value obtained by TEM.

ICP-OES was performed using a ICP Perkin Elmer optical emission spectrometer Optima 8000 to check the real metal loading. Au-Cu-supported samples were dissolved using a CEM MARS One Microwave Digester For alumina-supported samples, digestion was performed using an acidic solution of HCl (37%) and H_2SO_4 (98 %) in a 2:3 ratio at 180 °C (10 min temperature ramp—20 min maintenance—cooling down). For carbon-supported samples, the attack was performed with sulfonitric mixture (HNO_3:H_2SO_4 1:3) first, then Au was dissolved by aqua regia (HNO_3:HCl 1:3).

STEM-EDS composition measurements and spectrum imaging of the parent sols and the alumina-supported Au_1Cu_1 catalyst drop-dried on molybdenum microgrids were performed. For this, a FEI Titan Themis 200 kV Cs-corrected TEM transmission electron microscope (Eindoven, The Netherlands)

with 0.09 nm HRTEM and 0.16 nm STEM resolution equipped with 4 Thermofischer EDS detectors was applied. Measured data were evaluated and elemental maps were created by using the Velox software.

EDX spectra () recorded in 80–500 scans of selected area were cumulated, depending on the stability of the particles during the measurements. For Au and Cu elemental maps, background corrected and fit Au-L and Cu-K intensities, respectively, were applied. The Au/Cu atomic ratio was calculated for various particles on area localized on HAADF image that was measured simultaneously with the STEM-EDS measurements.

UV-visible spectra of the parent sols and the alumina-supported samples were recorded by an Agilent Cary 60 spectrometer (Santa Clara, C.A., USA) in transmission and diffuse reflectance mode, respectively, to measure the localized surface plasmon resonance (LSPR) of the Au-and Cu-containing nanoparticles.

X-ray photoelectron spectra (XPS) of the bimetallic samples were taken in an M-probe apparatus (Surface Science Instruments), for the determination of surface composition and oxidation state of the metals. The source was monochromatic Al K radiation (1486.6 eV). Data processing was performed by Esca Hawk software. The XPS lines of C 1s, O 1s, Au 4f and Cu 2p regions were recorded.

High angular annular dark field scanning transmission electron microscopy (HAADF-STEM) analysis was carried out using a ZEISS LIBRA200FE microscope equipped with a 200 kV FEG source. Before the analysis, the samples were finely smashed in an agate mortar, suspended in isopropanol and sonicated, then each suspension was dropped onto a lacey carbon-coated copper grid (300 mesh) and the solvent was evaporated. Histograms of the particle size distribution were obtained by counting onto the micrographs at least 300 particles. The mean particle diameter (d_m) was calculated by using the formula $d_m = \Sigma d_i n_i / \Sigma n_i$ where n_i was the number of particles of diameter d_i. The standard deviation was calculated by using the formula $SD = [\Sigma n_i (d_i - d_m)^2 / n_i]^{0.5}$.

The mono- and bimetallic Au-Cu catalysts were tested for the oxidation of 3,4-dimetoxybenzyl alcohol (veratryl alcohol, VA). Oxidation reactions were carried out in 100 mL stainless steel autoclave equipped with a glass inlet. In a typical experiment, 10 ml of a solution of veratryl alcohol in p-xylene (0.15 mol L^{-1}) and an appropriate amount of catalyst (VA:metal molar ratio 1000:1) were placed into the autoclave along with a magnetic stirrer. The system was flushed three times with O_2 first in order to remove any residual air in the atmosphere and then pressurized with 2 bar of O_2. The reaction was then heated at 80 °C and the solution stirred at a constant stirring rate of 1250 rpm. Samplings were carried out by stopping the stirring and quenching the reaction in an ice bath. A sample of solution was withdrawn and centrifuged in order to separate the catalyst. The products of reaction were identified by GC–MS (Thermo Scientific TRACE 1300 equipped with an Agilent HP-5 column, using undecane as external standard.

Recycling tests were carried out by recovering the catalyst after the reaction and re-using it without any further treatment with a fresh solution of VA.

4. Conclusions

Veratryl alcohol (VA) has been used as model for a lignin degradation product but also represents an important starting material for fragrances and additives, i.e., veratryl aldehyde. We report the study of AuCu bimetallic catalysts in the oxidation of VA using the sol immobilization technique. This latter technique was used for limiting differences in particle size by varying the Au/Cu ratio and the support. Indeed, we limited any difference in particle size within the series of catalysts prepared. We investigated Au/Cu molar ratios of 4, 1 and 0.25 using alumina and activated carbon as the support.

In the catalytic performance, we observed a strong dependence on the type of support used, being catalysts on Al_2O_3 definitely more active than the ones on carbon. UV-Vis and EDX analysis confirmed the bimetallic nature of the particles. In particular, Au_4Cu_1 and Au_1Cu_4 are, respectively, more rich in Au and Cu. XPS showed surface enrichment (even in different extents) of the major component and a higher metal exposure for Al_2O_3-supported catalysts. Moreover, the support effect was verified by comparing activities of catalysts with the same metal exposure. We also found that a linear correlation

can be established between conversion and gold surface exposure defining Au as the active phase. In particular, it was disclosed that Au^0 species is the active metal center of VA oxidation reaction. We concluded that the most active catalyst in VA oxidation was Au_4Cu_1 supported on Al_2O_3, even though the most stable appeared to be the Au_1Cu_1 one.

Supplementary Materials: The following are available online at http://www.mdpi.com/2073-4344/10/3/332/s1, Figure S1: Cu 2p deconvolution for (**A**) Au_4Cu_1 (**B**) Au_1Cu_1 and (**C**) Au_1Cu_4 C-supported catalysts, Figure S2: Cu 2p deconvolution for (**A**) Au_4Cu_1 (B) Au_1Cu_1 and (**C**) Au_1Cu_4 Al_2O_3-supported catalysts, Figure S3: Au 4f deconvolution for (**A**) Au_1Cu_1 (**B**) Au_4Cu_1 C-supported catalysts, Figure S4: Au 4f deconvolution for (**A**) Au_1Cu_1 (**B**) Au_4Cu_1 Al_2O_3-supported catalysts, Figure S5: Influence of (**A**) gold and (**B**) copper surface exposure on the conversion of VA after 1 h for Al_2O_3 supported catalysts, Figure S6: Influence of Au^0_{exp} exposure on the conversion at 1 h of reaction.

Author Contributions: Conceptualization, M.S. and A.V.; methodology, A.J.; validation, S.C. (Sofia Capelli), S.C. (Simone Cardaci); formal analysis, A.B. and G.S.; investigation, A.B. and M.S.; data curation, M.S. and S.C. (Simone Cardaci); writing—original draft preparation, M.S.; writing—review and editing, M.S., S.C. (Stefano Cattaneo) and L.P.; supervision, L.P.; project administration, L.P.; funding acquisition, L.P. and C.E. All authors have read and agreed to the published version of the manuscript.

Funding: This research received no external funding.

Acknowledgments: Authors gratefully acknowledge Gergely NAGY (Centre for Energy Research, Surface Chemistry and Catalysis Department, P.O. Box 49, Budapest H-1525, Hungary) for the preparation of the catalysts and for the UV-vis measurements. We also acknowledge the support of Hungarian national project VEKOP-2.3.3-15-2016-00002 (In the frame of this was purchased the Themis microscope).

Conflicts of Interest: The authors declare no conflict of interest.

References

1. Bruijnincx, P.C.A.; Weckhuysen, B.M. Lignin up for break-down. *Nat. Chem.* **2014**, *6*, 1035–1036. [CrossRef]
2. Heitner, C.; Schmidt, J.A.; Group, F. *Lignin and Lignans*; CRC Press: Boca Raton, FL, USA, 2016.
3. Zakzeski, J.; Bruijnincx, P.C.A.; Jongerius, A.L.; Weckhuysen, B.M. The catalytic valorization of lignin for the production of renewable chemicals. *Chem. Rev.* **2010**, *110*, 3552–3599. [CrossRef]
4. Wang, Z. Green Chemistry: Recent Advances in Developing Catalytic Processes in Environmentally-Benign Solvent Systems. Available online: http://ccc.chem.pitt.edu/wipf/frontiers/zhiyong.pdf (accessed on 1 February 2020).
5. Zakzeski, J.; Jongerius, A.L.; Weckhuysen, B.M. Transition metal catalyzed oxidation of Alcell lignin, soda lignin, and lignin model compounds in ionic liquids. *Green Chem.* **2010**, *12*, 1225–1236. [CrossRef]
6. Wu, X.; Guo, S.; Zhang, J. Selective oxidation of veratryl alcohol with composites of Au nanoparticles and graphene quantum dots as catalysts. *Chem. Commun.* **2015**, *51*, 6318–6321. [CrossRef]
7. Díaz-González, M.; Vidal, T.; Tzanov, T. Phenolic compounds as enhancers in enzymatic and electrochemical oxidation of veratryl alcohol and lignins. *Appl. Microbiol. Biotechnol.* **2011**, *89*, 1693–1700. [CrossRef] [PubMed]
8. Gutman, A.L.; Shkolnik, E.; Tishin, B.; Nisnevich, G. Process and Intermediates for Production of Donepezil and Related Compounds. U.S. Patent 6492522B1, 10 December 2002.
9. Lahtinen, P.; Korpi, H.; Haavisto, E.; Leskelä, M.; Repo, T. Parallel screening of homogeneous copper catalysts for the oxidation of benzylic alcohols with molecular oxygen in aqueous solutions. *J. Comb. Chem.* **2004**, *6*, 967–973. [CrossRef] [PubMed]
10. Mate, V.R.; Shirai, M.; Rode, C.V. Heterogeneous Co3O4 catalyst for selective oxidation of aqueous veratryl alcohol using molecular oxygen. *Catal. Commun.* **2013**, *33*, 66–69. [CrossRef]
11. Melián-Rodríguez, M.; Saravanamurugan, S.; Kegnæs, S.; Riisager, A. Aerobic Oxidation of Veratryl Alcohol to Veratraldehyde with Heterogeneous Ruthenium Catalysts. *Top. Catal.* **2015**, *58*, 1036–1042. [CrossRef]
12. Stucchi, M.; Cattaneo, S.; Cappella, A.; Wang, W.; Wang, D.; Villa, A.; Prati, L. Catalytic Oxidation of Methoxy Substituted Benzyl Alcohols as Model for Lignin Valorisation. *Catal. Today* **2019**. [CrossRef]
13. Olmos, C.M.; Chinchilla, L.E.; Cappella, A.M.; Villa, A.; Delgado, J.J.; Hungría, A.B.; Blanco, G.; Calvino, J.J.; Prati, L.; Chen, X. Selective oxidation of veratryl alcohol over Au-Pd/Ce0.62Zr0.38O2 catalysts synthesized by sol-immobilization: Effect of Au:Pd molar ratio. *Nanomaterials* **2018**, *8*, 669. [CrossRef]
14. Haruta, M.; Kobayashi, T.; Sano, H.; Yamada, N. Novel Gold Catalysts for the Oxidation of Carbon Monoxide at a Temperature far Below 0 °C. *Chem. Lett.* **1987**, *16*, 405–408. [CrossRef]

15. Hutchings, G.J. Vapor phase hydrochlorination of acetylene: Correlation of catalytic activity of supported metal chloride catalysts. *J. Catal.* **1985**, *96*, 292–295. [CrossRef]
16. Silva, T.A.G.; Teixeira-Neto, E.; López, N.; Rossi, L.M. Volcano-like behavior of Au-Pd core-shell nanoparticles in the selective oxidation of alcohols. *Sci. Rep.* **2014**, *4*, 5766. [CrossRef] [PubMed]
17. Cattaneo, S.; Stucchi, M.; Villa, A.; Prati, L. Gold Catalysts for the Selective Oxidation of Biomass-Derived Products. *ChemCatChem* **2019**, *11*, 309–323. [CrossRef]
18. Schwank, J. Gold in bimetallic catalysts. *Gold Bull.* **1985**, *18*, 2–10. [CrossRef]
19. Markó, I.E.; Giles, P.R.; Tsukazaki, M.; Brown, S.M.; Urch, C.J. Copper-catalyzed oxidation of alcohols to aldehydes and ketones: An efficient, aerobic alternative. *Science* **1996**, *274*, 2044–2046. [CrossRef]
20. Albadi, J.; Alihoseinzadeh, A.; Razeghi, A. Novel metal oxide nanocomposite of Au/CuO–ZnO for recyclable catalytic aerobic oxidation of alcohols in water. *Catal. Commun.* **2014**, *49*, 1–5. [CrossRef]
21. Zhan, W.; Wang, J.; Wang, H.; Zhang, J.; Liu, X.; Zhang, P.; Chi, M.; Guo, Y.; Guo, Y.; Lu, G.; et al. Crystal Structural Effect of AuCu Alloy Nanoparticles on Catalytic CO Oxidation. *J. Am. Chem. Soc.* **2017**, *139*, 8846–8854. [CrossRef]
22. Destro, P.; Marras, S.; Manna, L.; Colombo, M.; Zanchet, D. AuCu alloy nanoparticles supported on SiO2: Impact of redox pretreatments in the catalyst performance in CO oxidation. *Catal. Today* **2017**, *282*, 105–110. [CrossRef]
23. Della Pina, C.; Falletta, E.; Rossi, M. Highly selective oxidation of benzyl alcohol to benzaldehyde catalyzed by bimetallic gold-copper catalyst. *J. Catal.* **2008**, *260*, 384–386. [CrossRef]
24. Marelli, M.; Jouve, A.; Villa, A.; Psaro, R.; Balerna, A.; Prati, L.; Evangelisti, C. Hybrid Au/CuO Nanoparticles: Effect of Structural Features for Selective Benzyl Alcohol Oxidation. *J. Phys. Chem. C* **2019**, *123*, 2864–2871. [CrossRef]
25. Liu, X.; Wang, A.; Li, L.; Zhang, T.; Mou, C.-Y.; Lee, J.-F. Structural changes of Au–Cu bimetallic catalysts in CO oxidation: In situ XRD, EPR, XANES, and FT-IR characterizations. *J. Catal.* **2011**, *278*, 288–296. [CrossRef]
26. Amendola, V.; Pilot, R.; Frasconi, M.; Maragò, O.M.; Iatì, M.A. Surface plasmon resonance in gold nanoparticles: A review. *J. Phys. Condens. Matter* **2017**, *29*, 203002. [CrossRef] [PubMed]
27. Daniel, M.C.; Astruc, D. Gold Nanoparticles: Assembly, Supramolecular Chemistry, Quantum-Size-Related Properties, and Applications Toward Biology, Catalysis, and Nanotechnology. *Chem. Rev.* **2004**, *104*, 293–346. [CrossRef] [PubMed]
28. Creighton, J.A.; Eadon, D.G. Ultraviolet–visible absorption spectra of the colloidal metallic elements. *J. Chem. Soc. Faraday Trans.* **1991**, *87*, 3881–3891. [CrossRef]
29. Lisiecki, I.; Pileni, M.P. Copper metallic particles synthesized "in situ" in reverse micelles: Influence of various parameters on the size of the particles. *J. Phys. Chem.* **1995**, *99*, 5077–5082. [CrossRef]
30. Luo, Y.; Tu, Y.; Ren, Q.; Dai, X.; Xing, L.; Li, J. Surfactant-free fabrication of Cu_2O nanosheets from Cu colloids and their tunable optical properties. *J. Solid State Chem.* **2009**, *182*, 182–186. [CrossRef]
31. Xu, Z.; Lai, E.; Yang, S.H.; Hamad-Schifferli, K. Compositional dependence of the stability of AuCu alloy nanoparticles. *Chem. Commun.* **2012**, *48*, 5626–5628. [CrossRef]
32. Wang, H.; Liu, D.; Xu, C. Directed synthesis of well dispersed and highly active AuCu and AuNi nanoparticle catalysts. *Catal. Sci. Technol.* **2016**, *6*, 7137–7150. [CrossRef]
33. Schünemann, S.; Dodekatos, G.; Tüysüz, H. Mesoporous Silica Supported Au and AuCu Nanoparticles for Surface Plasmon Driven Glycerol Oxidation. *Chem. Mater.* **2015**, *27*, 7743–7750. [CrossRef]
34. Casanova, O.; Iborra, S.; Corma, A. Biomass into chemicals: Aerobic oxidation of 5-hydroxymethyl-2-furfural into 2,5-furandicarboxylic acid with gold nanoparticle catalysts. *ChemSusChem.* **2009**, *2*, 1138–1144. [CrossRef] [PubMed]
35. Albonetti, S.; Pasini, T.; Lolli, A.; Blosi, M.; Piccinini, M.; Dimitratos, N.; Lopez-Sanchez, J.A.; Morgan, D.J.; Carley, A.F.; Hutchings, G.J.; et al. Selective oxidation of 5-hydroxymethyl-2-furfural over TiO 2-supported gold-copper catalysts prepared from preformed nanoparticles: Effect of Au/Cu ratio. *Catal. Today* **2012**, *195*, 120–126. [CrossRef]
36. Moore, A.D.; Holmes, S.M.; Roberts, E.P.L. Evaluation of porous carbon substrates as catalyst supports for the cathode of direct methanol fuel cells. *RSC Adv.* **2012**, *2*, 1669–1674. [CrossRef]